JOURNAL OF MATERIALS SCIENCE 31 (1996) 6455–6461

High-strain fatigue of Pb–Sn eutectic solder alloy

H. JIANG, R. HERMANN†, W. J. PLUMBRIDGE
Materials Department, The Open University, Milton Keynes MK7 6AA, UK

Low-cycle fatigue of tin–lead eutectic solder was studied at room temperature. The responding load level under cyclic strain was found to decrease continually with number of cycles and this behaviour was described by a constitutive equation. No significant difference in fatigue behaviour was observed between the tests with $R = -1$ and $R = 0$ ($R = \varepsilon_{min}/\varepsilon_{max}$) under the same strain amplitude, and this was attributed to the high level of plastic strain produced. Multiple initiation of fatigue cracks was promoted by slip bands developed on the surface of the specimen.

1. Introduction

In electronic application, surface-mounted components are increasingly being used [1], where the mounting of the device is directly soldered to pads on printed wiring board without leads. This technology reduces both the size and weight of the final circuit board, enhances circuit operation and reduces production costs. Unfortunately, with surface mounting there is no lead to flex and absorb thermal and mechanical strains. The solder in a surface-mounted component is, therefore, vulnerable to damage from this source. It is well known that the thermal strains in chip carriers can be large when temperature variations occur during service, owing to difference between the coefficients of thermal expansion of the carrier and the substrate material. Failure of solder joints is recognized as a major cause of failure of components. For many electronic devices, safe performance is required and failures due to the thermomechanical fatigue in chip carries must be avoided by appropriate design, by matching carrier and substrate materials, and by the appropriate selection of solder. However, thermomechanical fatigue is difficult to study because there is a change in the properties of the solder as the temperature changes [2]. Instead, isothermal fatigue study is usually performed in the strain and temperature ranges of interest to form a basis for understanding thermal fatigue properties.

As for most metals [3, 4], many (tin–lead) Sn–Pb solders obey the Coffin–Manson low-cycle fatigue law [5–9], in which the fatigue life, N_f, is a function of the applied plastic strain range, $\Delta\varepsilon_p$, in the form

$$N_f^{\alpha}\Delta\varepsilon_p = \theta \quad (1)$$

Where α and θ are constants.

For the near eutectic 60Sn–40Pb solder tested in shear from 1%–10% plastic strain range at a frequency of 0.3 Hz and −50–150 °C, the Coffin–Manson exponent, α, has been found to vary from 0.52–0.90 at 35 °C, depending on the load drop and definition of fatigue life used [5]. If the fatigue life is defined as the number of cycles needed to reduce the hysteresis load range to one-half its maximum value, α is 0.59. A different observation was reported for the same solder (60Sn–40Pb) between 20 and 70 °C [6]. The plastic strain range versus number of cycles to failure plot was basically a straight line which validated the Coffin–Manson relationship, but the definition of fatigue life percentage of load reduction from 5% to 50% had little effect on α value.

During fatigue under strain control, Sn–Pb solder usually exhibits a continuous decrease in hysteresis load with the number of cycle [6, 9, 10]. Solomon [9, 11] indicated that the decrease in hysteresis load correlated with the development and growth of fatigue cracks and could be used as a measure of fatigue cracking and failure. It was reported that cracks could be observed as early as 10% load drop [6]. A load drop is then employed to define the fatigue life, but a different load drop can significantly influence the fatigue life [5, 6, 9, 10]

Many studies on the fatigue of Sn–Pb solder joints have been reported [2, 5–12]. However, little data are available in the literature on fatigue properties of the solder materials themselves. This work aimed to investigate isothermal low-cycle fatigue behaviour of cast Sn–Pb eutectic alloy in bulk specimens. The load change behaviour during a fatigue test, the effect of mean strain on fatigue life and fatigue fracture characteristics were considered. The fatigue properties of the present study are compared with those provided from literature sources on solder joint specimens.

2. Experimental procedures

The material used was a commercial grade eutectic 63Sn–37Pb alloy which is the most widely used solder material within the electronics manufacturing industry. The alloy was supplied in rectangular bar form. The alloy bars were then remelted and cast into preheated (185 °C) aluminium moulds. The moulds were rapidly quenched in cold water. The cast specimens

† Deceased

0022–2461

were ready for testing without further machining and stored in a freezer at $-24\,^{\circ}C$ to minimize natural ageing. A specimen was removed from the freezer about 15 h before testing. The specimen was cylindrical with a guage length of 25 mm and a diameter of 11.28 mm.

All fatigue tests were carried out under total strain control on a servo-hydraulic testing machine at room temperature. The strain was measured by a strain-guage extensometer which was attached to the specimen within the gauge length. Cosidering the fact that the deformation behaviour of Pb–Sn solder was highly strain-rate dependent [9, 13], all fatigue tests were performed at a constant strain rate of $3.33 \times 10^{-3}\ s^{-1}$. This means that the cycling frequency varied from test to test, depending on the total strain range which was used as a control limit. The total strain range varied from 0.5%–3% strain in this study. A triangular wave form was selected for the fatigue tests with the strain ratio, R, at $R = -1$ and 0.

Scanning electron microscopy (SEM) and optical techniques were used to examine the alloys after fracture. The samples were cut from both untested and failed specimens along the cross-section and longitudinal directions within the gauge length. The fracture surface of failed specimens was also examined to determine the fatigue fracture characteristics and mechanism of failure of the solder.

3. Results

3.1. Hysteresis behaviour

The load and total displacement were measured in each test by an X–Y chart recorder to display the hysteresis loops. The typical appearance of such hysteresis loops at low and high strain ranges is shown in Fig. 1. The load changed drastically with strain at low strain amplitude but saturation of the hysteresis load occurred at high strain ranges (Fig. 1b). A cyclic stress–strain curve constructed from the first cycle load data is plotted in log $\Delta\sigma$–log $\Delta\varepsilon$ coordinates (Fig. 2), and may be described by

$$\Delta\sigma = A\Delta\varepsilon^{\beta} \qquad (2)$$

where $\Delta\sigma$ is the stress range at the first cycle, $\Delta\varepsilon$ is the total strain range and A (= 130.8) and β (= 0.09) are constants.

An X–T chart was used for the continuous monitoring of the load level. Fig. 3 shows the variation in peak tensile load, peak compressive load and load range (sum of absolute value of tensile and compressive load) for a test at a strain range of 2%. The load levels decreased continuously from the first cycle, and the peak tensile and compressive loads were almost identical. Initially, the load reduction was rapid, then fairly constant and finally accelerated. This load drop can be described by a parameter, ϕ, which is defined as

$$\phi = 1 - (\Delta P/\Delta P_m) \qquad (3)$$

where ΔP is the load range at any cycle number and ΔP_m is the maximum load range which was observed at the first cycle. Fig. 4 shows load-drop parameter

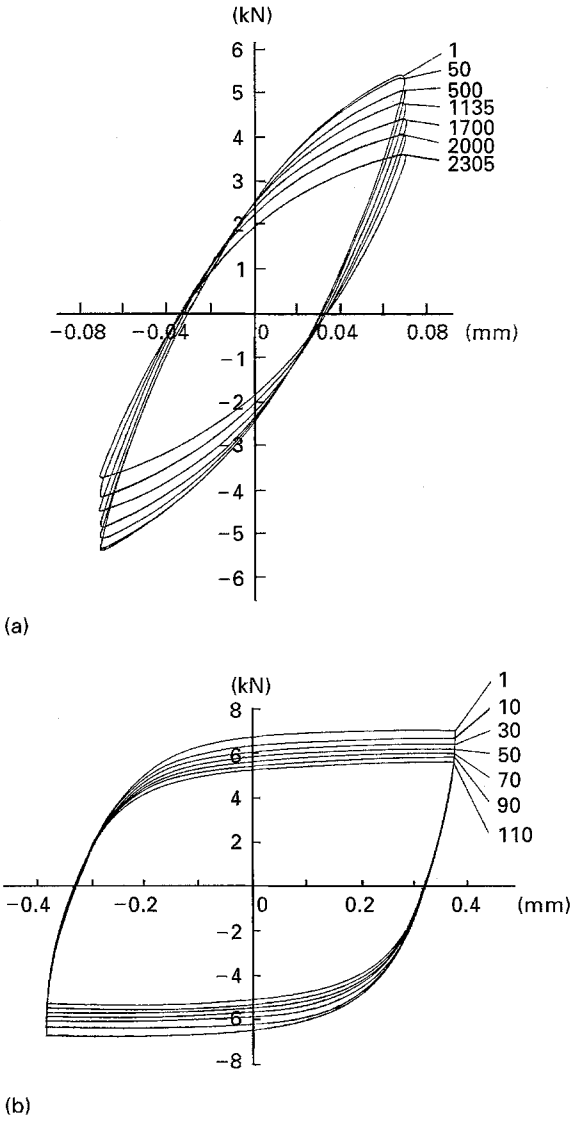

Figure 1 Experimental load–displacement hysteresis loops at total strain range of (a) 0.56% and (b) 3%.

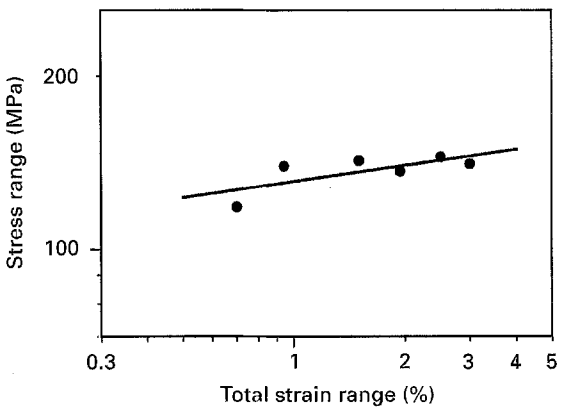

Figure 2 Cyclic stress–strain behaviour of eutectic Sn–Pb alloy: (●) measured, (—) fitted.

curves for all strain ranges tested, and the three stage behaviour is apparent.

3.2. Fatigue behaviour

To investigate the effect of failure definition, load-drop values of 5%, 10%, 15%, 20%, 25% and 30% were selected and the corresponding fatigue life curves are

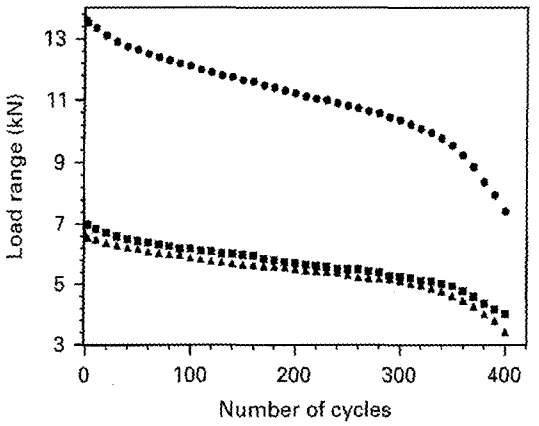

Figure 3 Load range level as a function of cyclic number at total strain range 2.0% and $R = -1$. (▲) Tensile load, (■) compressive load, (●) load range.

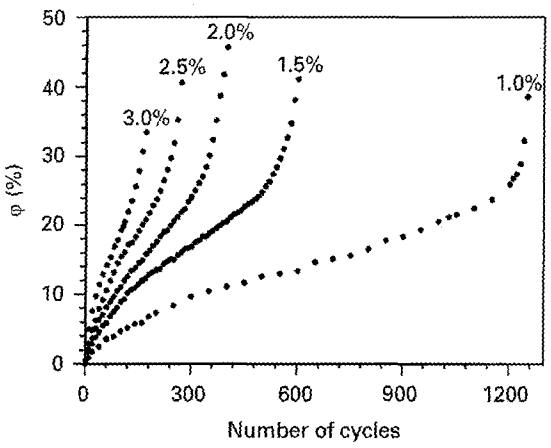

Figure 4 Load-drop parameter as a function of cyclic number. The numbers over the curves are strain ranges.

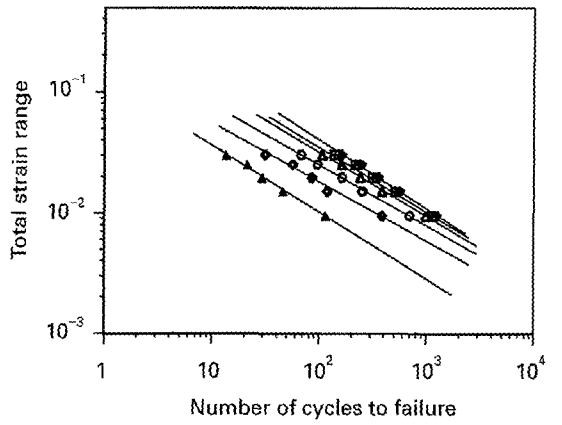

Figure 5 Fatigue life defined by (▲) 5%, (◇) 10%, (○) 15%, (△) 20%, (⊞) 25% and (◆) 30% load drop. α: (▲) 0.56, (◇) 0.48, (○) 0.50, (△) 0.53, (⊞) 0.56, (◆) 0.57. Room temperature; $\dot{\varepsilon} = 3.3 \times 10^{-3}\ s^{-1}$.

shown in Fig. 5. There is essentially a linear relationship between fatigue life and total strain range on the double logarithmic scale for all definitions of failure. The fatigue life curves are basically parallel. The slopes, α, were measured as 0.56, 0.48, 0.50, 0.53, 0.56 and 0.57 corresponding to 5%, 10%, 15%, 20%, 25%, 30% load drop, indicating that the Coffin–Manson slope is virtually independent of the definition of failure although the different definitions resulted in an apparent difference of fatigue life.

Some fatigue tests were performed with a strain ratio $R = 0$, i.e. the minimum strain was zero and the maximum strain was twice the strain amplitude. An interesting observation is that the mean strain, although as large as the strain amplitude, did not cause a significant mean stress. When the total strain varied from zero to maximum value and then back to zero, the corresponding load level increased from zero to the maximum and then continuously decreased until it created a negative load with nearly the same value as the peak positive load level, i.e. the mean load was almost zero. Fig. 6 shows the peak tensile load, peak compressive load and mean load recorded during a test for a total strain range of 2%. It can be seen that there is little difference between tensile and compressive load and the mean load is nearly zero throughout the whole fatigue test despite a mean strain of 1%. The fatigue life tested at $R = 0$ was compared with that at $R = -1$ under the same strain amplitude. No significant difference was observed (Fig. 7).

To investigate the effect of specimen geometry, a comparison was made between the present data and those available in the literature for the same or similar solder materials (Fig. 8). The details of test conditions and results are listed in Table 1. While a direct comparison between these data is difficult due to different testing conditions and methods, the agreement in the

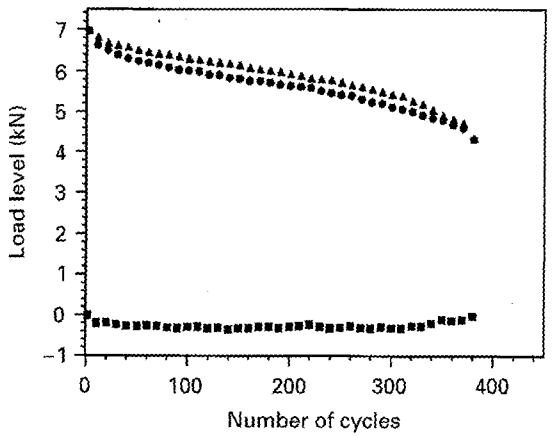

Figure 6 Load level as a function of cyclic number at a total strain of 2%, $R = 0$. (●)Tensile load, (▲) compressive load (■) mean load.

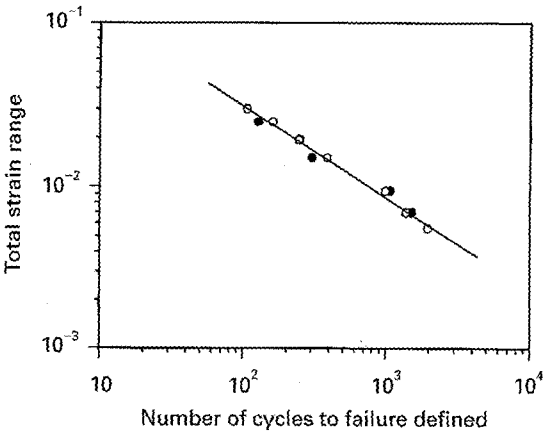

Figure 7 Fatigue life versus strain range for tests of R(○) $= -1$ and (●) $= 0$. 20% load drop, $\dot{\varepsilon} = 0.0033\ s^{-1}$, $\alpha = 0.54$.

TABLE I Fatigue test parameters for curves in Fig. 8

Materials	Specimen	Strain mode	Load mode	Failure definition	f (Hz)	$\dot{d}^a/\dot{\varepsilon}$ $(\mu ms^{-1})/(s^{-1})$	α	Ref
60Sn–40Pb	Solder joint	Plastic strain	Shear	50% load drop	0.3		0.52	[2]
60Sn–40Pb	Solder joint	Plastic strain	Shear	20% load drop		0.32[a]	0.55[b]	[6]
60Sn–40Pb	Solder joint	Plastic strain	Shear	50% load drop	0.5		0.52	[8]
60Sn–40Pb	Solder joint	Total strain	Shear	30% load drop		0.83[a]	0.18[b]	[16]
63Sn–37Pb	Solder joint	Plastic strain	Shear		0.1		0.35[b]	[10]
63Sn–37Pb	Bulk Specimen	Total strain	Pull-Push	20% load drop		3.3×10^{-3}	0.53	Author's data

[a] Displacement rate
[b] Graphically estimated values.

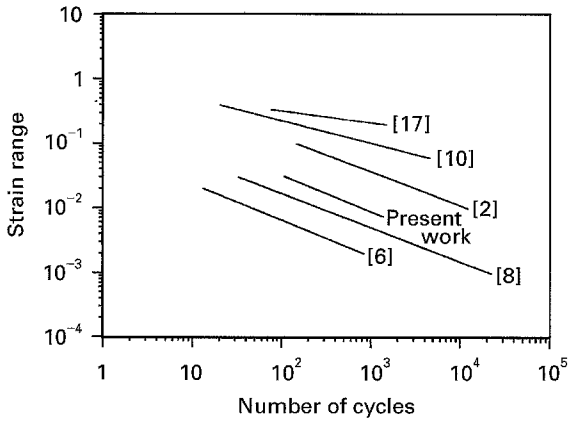

Figure 8 Comparison of fatigue life from different sources.

α values in Fig. 8 suggests that while there is a similarity between some data sets, others exhibit a marked variance in fatigue behaviour between bulk and joint specimen geometries. Fig. 8 also shows a significant difference in fatigue life between the data, even between those with the same specimen geometry of solder joint. The possible causes for this difference will be discussed later.

3.3. Fatigue fracture

Fatigue cracks were observed on the surface under all strain ranges investigated. These cracks were found to initiate and grow along slip bands. Fig. 9 shows several cracks developed along slip bands at about 45° to the axis of the applied stress. At lower strain ranges, the number of cracks was less and the slip bands were finer.

Cracks often initiated at different sites on the surface and grew simultaneously into the body of the specimen. Some cracks then linked up with each other to cause fast growth and final failure. This fracture process can be seen clearly on the fracture surface of failed specimens (Fig. 10). The radial shear ridges indicated several initial sites and the fracture was caused by growth of cracks from these sites. There was little evidence of striations.

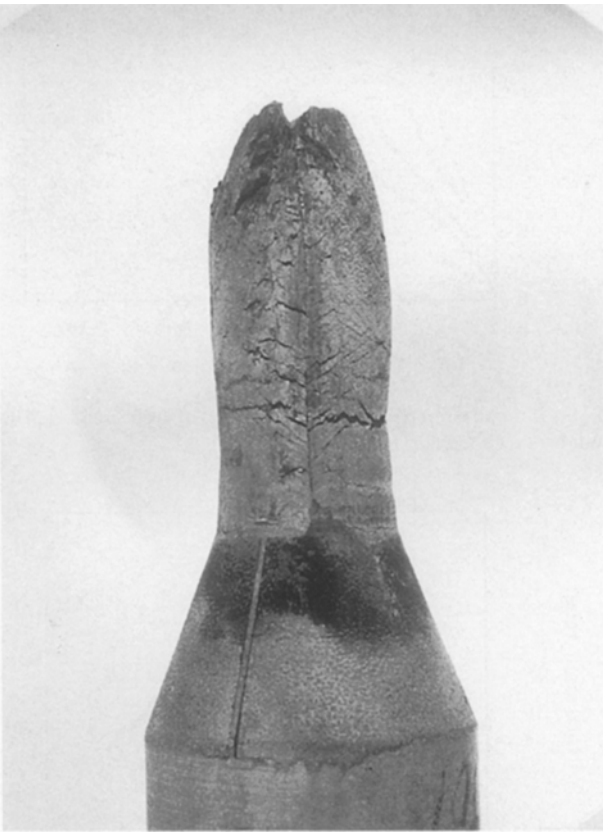

Figure 9 Optical photograph showing cracks on the surface of failed specimen tested at strain range of 3%.

Examination of the longitudinal section of the gauge length shows that cracks formed on the surface of the specimen grew initially along the slip plane as far as about 100 μm and then propagated along the plane perpendicular to the applied stress axis as shown in Fig. 11. The fracture path was predominantly transgranular through the tin-rich matrix. Lead-rich particles were occasionally cut.

4. Discussion

The eutectic solder exhibited cyclic softening behaviour at both low and high strain ranges. Under strain-control cycling the corresponding load levels may

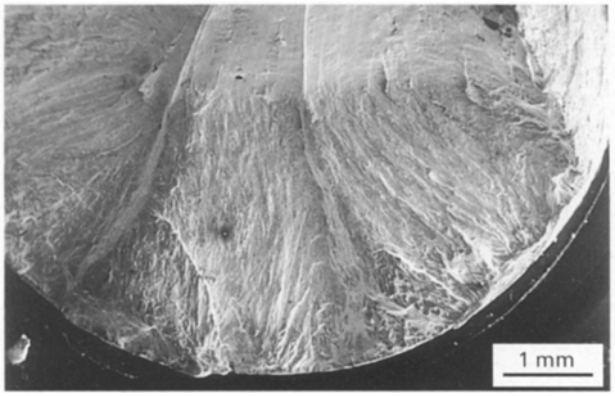

Figure 10 Scanning electron micrograph showing fracture surface of a failed specimen tested at strain range of 1%.

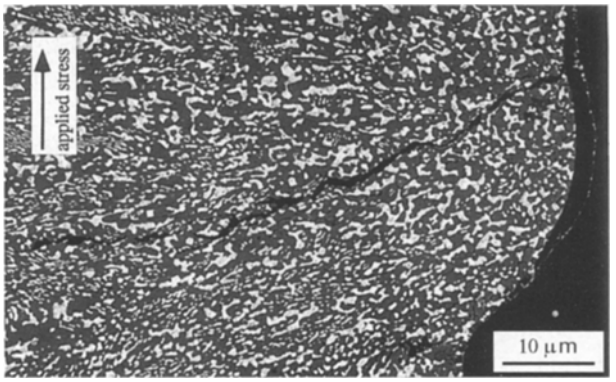

Figure 11 Scanning electron micrograph showing cracks on the longitudinal section of a failed specimen tested at strain range of 3%.

increase, decrease or remain essentially unchanged with number of cycles [14]. A decrease in load level could be caused either by a change in microstructure, which does not alter the load-bearing area, or by cavity formation and fatigue crack nucleation, which do reduce the load-bearing area. Solomon [11] indicated that load drop, due to microstructural change, occurs at the beginning of a fatigue test but then quickly saturates. The saturation is marked by a plateau where there is little or no further drop in load until crack growth becomes influential. In the present study, the load drop occurred from the first cycle and was continuous without any plateau being reached, indicating that the reduction in the load-bearing area due to fatigue cracking is a dominant cause for the observed decrease of load level. It is argued that the load drop is primarily a measure of fatigue cracking. The onset of fatigue crack growth of a certain length is often used to define the fatigue life. However, it is difficult to measure the fatigue crack length due to multiple nucleation and irregular growth [11]. The load drop, which reflects the fatigue cracking process, is easily recorded throughout a fatigue test. Therefore, it would be very useful for the determination and prediction of fatigue life if the load-drop behaviour and its relationship with strain range could be quantitatively described.

Crack initiation and growth result in a variation of load drop (Figs 3 and 4) in the three-stage manner previously described. The process can be described by a three-term function in the form of

$$\phi = x_1 N^{1/3} + x_2 N + x_3 N^3 \quad (3)$$

where x_i ($i = 1$–3) are coefficients and N is the number of cycles. An example is given in Fig. 12 showing the experimental points and the curve fitted by Equation 3 for a strain range of 3%. It can be seen that there is good agreement between the experimental data and the fitted curve. The three coefficients can be correlated with the strain range. Fig. 13 shows that x_i ($i = 1$, 2, 3) exhibits a linear relationship with the strain range $\Delta\varepsilon$ in a double-log plot, i.e.

$$x_1 = 1.163\ (\Delta\varepsilon)^{0.658} \quad (4a)$$

$$x_2 = 3.39 \times 10^{-3}\ (\Delta\varepsilon)^{2.54} \quad (4b)$$

$$x_3 = 8.22 \times 10^{-9}\ (\Delta\varepsilon)^{4.91} \quad (4c)$$

For a given strain range, the coefficients, x_i ($i = 1, 2, 3$), can be determined using Equation 4. Substituting these coefficients into Equation 3, a relationship between load drop and number of cycles is determined and hence a load-drop curve can be drawn. Fatigue life can then be predicted from these curves by providing a value of ϕ for the failure definition. Fig. 14 shows the fatigue life curves predicted by this method. It should be noted that a limited number of data at low strain ranges are required to validate and refine the prediction.

While a load drop is usually used for the definition of failure in the case of continuous reduction of load level, the fatigue life can be defined at any load drop. Fig. 5 demonstrates that different definitions for fatigue failure in terms of load drop did not cause significant change in the Coffin–Manson slope, α. Similar behaviour was reported by Sandström *et al.* [6] on the solder 60Sn–40Pb. These authors presented fatigue-life curves which were essentially parallel. However, contrary observations on the effect of failure definition on the Coffin–Manson slopes have been reported for the same solder. For example, Solomon [5] showed a strong influence of failure definitions on Coffin–Manson slope. The value of α decreased from 0.90 to 0.52 when the failure definition increased from 10% to 90% load drop. Despite this controversy, the

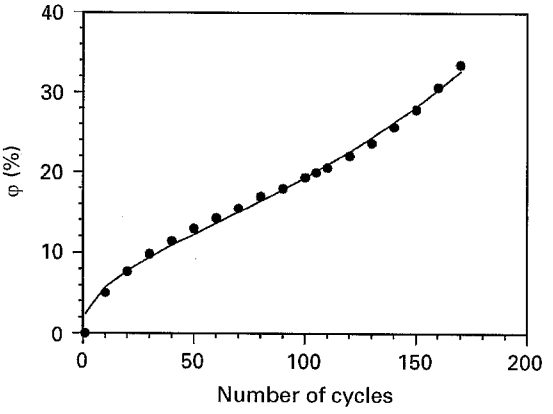

Figure 12 (●) Experimental points of load drop and (—) fitted curve at a total strain range of 3%.

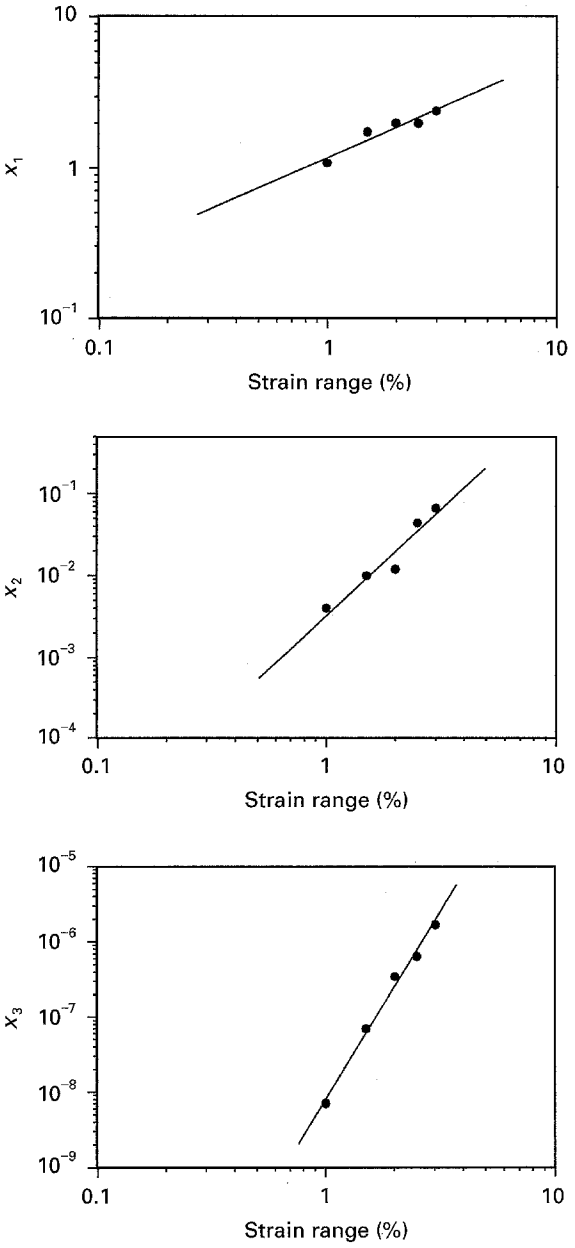

Figure 13 Coefficients in Equation 3 as a function of strain range. (a) $x_1 = 1.163(\Delta\varepsilon)^{0.658}$; (b) $x_2 = 3.39 \times 10^{-3}(\Delta\varepsilon)^{2.54}$; (c) $x_3 = 8.22 \times 10^{-9}\ (\Delta\varepsilon)^{4.91}$. (●) Measured, (—) fitted.

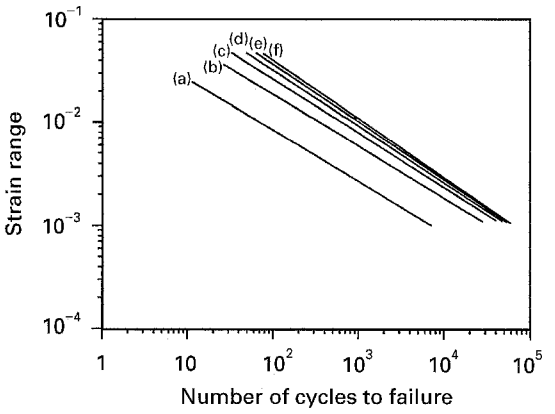

Figure 14 Fatigue-life curve predicted by Equations 3 and 4. Failure defined with a load drop of (a) 5%, (b) 10%, (c) 15%, (d) 20%, (e) 25% and (f) 30%.

average value of 0.53 for the Coffin–Manson exponent measured in the present case is in good agreement with the results of most research on Pb–Sn solder [2, 5, 6, 8–12].

As mentioned above, the mean strain (at $R = 0$), although as high as the strain amplitude, did not cause a significant mean stress (Fig. 6) and the stress response was the same as that at $R = -1$ (Fig. 3). In such low-strength material, the plastic strain dominates the total strain which was used for the strain control limit. If the elastic strain accounted for a significant portion of the total strain, the peak compressive load would be lower than the peak tensile load due to the relaxation of elastic load when the elastic strain recovered. The resulting similarity in the hysteresis loops explains the coincidence in endurance (Fig. 7).

The present fatigue tests were performed using bulk specimens to provide an understanding of the mechanical behaviour of solder material itself which is required for improving performance and developing reliable methods of life prediction. Fig. 8 shows a significant difference of fatigue life between the present data and data obtained using solder joint specimens. This cannot be attributed solely to the difference in specimen geometries because a wide variation exists between the joints themselves (Fig. 8). Possible reasons for this wide divergence of data include inconsistent definitions of failure, variations in strain rate during cycling and the differences arising between alternating shear strain in the joints and fluctuating tension–compression in the present study. It has been reported that various definitions of failure lead to different fatigue life [5, 6, 9, 10] and reduction in strain rate results in a decrease of fatigue life [10, 12, 15]. A fatigue test in tension–compression is not equivalent to that in shear at the same strain range. About twice the strain range is required to produce the same damage in shear fatigue as that in tensile fatigue [10]. In spite of this divergence, it is not difficult to see from Fig. 8 that the present data fall within the data presented by others using solder joint geometries.

5. Conclusions

1. Low-cycle fatigue was performed on Sn–Pb eutectic solder alloy at room temperature. Under total strain control, the load continuously decreased from the first cycle at all strain ranges studied. Cyclic softening is attributed to the initiation and growth of fatigue cracks.

2. The load-drop curve exhibited three stages and could be described by a constitutive equation

$$\phi = x_1 N^{1/3} + x_2 N + x_3 N^3 \quad (3)$$

where ϕ and N are load-drop parameter and number of cycles, respectively. The three coefficients (x_i, $i = 1$, 2, 3) are the function of strain range in the form

$$x_1 = 1.163(\Delta\varepsilon)^{0.658} \quad (4a)$$

$$x_2 = 3.39 \times 10^{-3}(\Delta\varepsilon)^{2.54} \quad (4b)$$

$$x_3 = 8.22 \times 10^{-9}(\Delta\varepsilon)^{4.91} \quad (4c)$$

3. For the fatigue tests with strain ratio $R = 0$, the maximum compressive load was almost identical to the maximum tensile load, that is, the mean load was about zero despite a mean strain as large as the strain amplitude. This is due to the high level of plastic strain created during cycling and which constituted the overwhelming proportion of the total strain. No significant difference in fatigue life was observed between the tests with $R = -1$ and $R = 0$ under the same strain amplitude because the hysteresis loops were virtually identical.

4. Fatigue cracks developed along slip bands on the surface of specimen. The fracture path was predominantly through the tin-rich matrix with lead-rich particles occasionally cut.

5. The present fatigue data were compared with those in the literature obtained on solder joint specimens. Values of the Coffin–Manson exponent were in good agreement, but significant differences in fatigue life were apparent and this divergence was tentatively attributed to differences in failure definition, strain rate and loading mode.

Acknowledgements

The authors acknowledge the use of the laboratory facilities at the Materials Department in the Open University, particularly the collaboration of P. Ledgard for specimen production and J. Moffatt for providing technical support.

References

1. J. H. LAU and D. W. RICE, *Solid State Technol.* **28** (1985) 91.
2. H. D. SOLOMON, *IEEE Trans. Compon. Hybrids Manuf. Technol.* **CHMT-9** (1984) 423.
3. L. F. COFFIN, *Trans. ASME* **76** (1954) 931.
4. S. S. MANSON, *Exp. Mech.* **5** (1965) 193.
5. H. D. SOLOMON, *J. Electron. Packaging* **111** (1989) 75.
6. R. SANDSTRÖM, J.-O. ÖSTERBERG and M. NYLÈN, *Mater. Sci. Technol.* **9** (1993) 811.
7. G. ENGBERG, L. E. LARSSON, M. NYLEN and H. STEEN, *Brazing Soldering* **11** (1986) 62.
8. N. F. ENKE, T. J. KILINSKI, S. A. SCHROEDER and J. R. LESNIAK, in "Proceedings of 39th Electronic Components Conference" (IEEE, Piscataway, NJ, 1989) p. 264.
9. H. D. SOLOMON, *J. Electron. Packaging* **113** (1991) 102.
10. S. VAYNMAN, M. E. FINE and D. A. JEANNOTTE in "Solder Mechanics–A state of the Art Assessment" (Minerals, Metals and Materials Society, 1991) p. 155.
11. H. D. SOLOMON, "Electronic Packaging—Materials and Processes" (ASM, 1986) p. 29.
12. H. D. SOLOMON, in "Low Cycle Fatigue", ASTM STP 942 (American Society for Testing and Materials, Philadelphia, PA, 1988) p. 342.
13. K. KAWASHIMA, T. ITO and M. SAKURAGI, *J. Mater. Sci.* **27** (1992) 6387.
14. E. A. STRAKE Jr, in "Fatigue and Microstructure" (ASM, OH, 1979) p. 205.
15. S. VAYNMAN, *IEEE Trans. Comp. Hybrids Manuf. Technol.*, **12** (1989) 469.
16. N. R. BONDA and I. C. NOYAN *Metall. Trans.* **23A** (1992) 479.
17. D. FREAR, D. GRIVAS, M. McCORMACK, D. TRIBULA and J. W. MORRIS Jr, in "Proceedings of Symposium on Effects of load and Thermal Histories on Mechanical Behaviour" (1987) p. 113.

Received 20 October
and accepted 20 November 1995